iScience

Article

# Spine loss in depression impairs dendritic signal integration in human cortical microcircuit models

## Graphical abstract

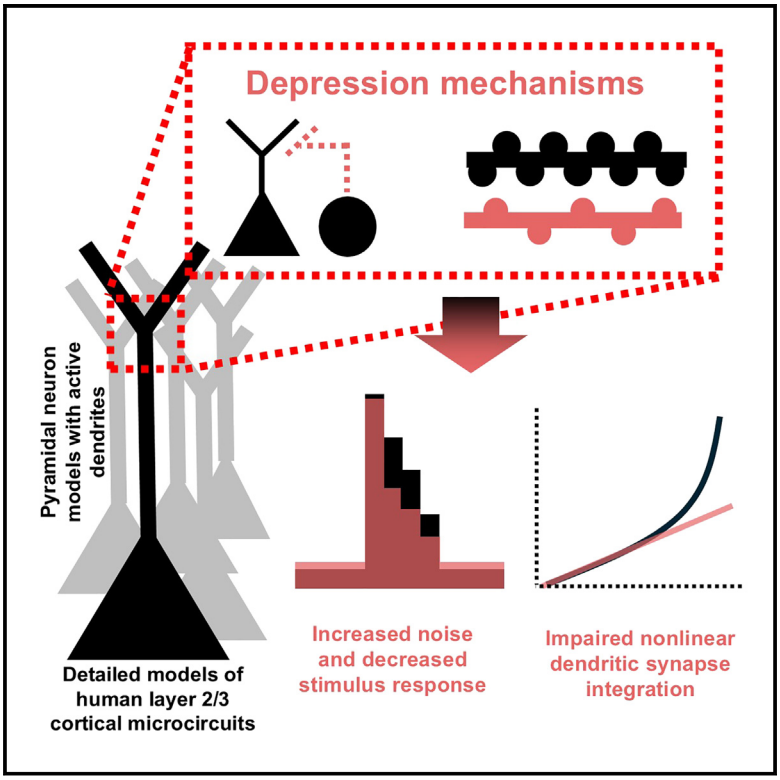


## Authors

Heng Kang Yao, Frank Mazza, Thomas D. Prevot, Etienne Sibille, Etay Hay

## Correspondence

etay.hay@camh.ca

## In brief

Neuroscience; Sensory neuroscience; Depression; Dendrites

## Highlights

- Detailed biophysical models of human cortical microcircuits with active dendrites
- Spine loss in depression decreases response and impairs signal detection
- Spine loss abolishes nonlinear dendritic integration

Yao et al., 2025, iScience *28*, 112136
May 16, 2025 
https://doi.org/10.1016/j.isci.2025.112136

CellPress

iScience

CellPress
OPEN ACCESS

Article

# Spine loss in depression impairs dendritic signal integration in human cortical microcircuit models

Heng Kang Yao,[1,2] Frank Mazza,[1,2] Thomas D. Prevot,[3,4] Etienne Sibille,[3,4,5] and Etay Hay[1,2,3,6,*]
[1]Krembil Centre for Neuroinformatics, Centre for Addiction and Mental Health, Toronto, ON M5T 1R8, Canada
[2]Department of Physiology, University of Toronto, Toronto, ON M5S 1A1, Canada
[3]Department of Psychiatry, University of Toronto, Toronto, ON M5S 1A1, Canada
[4]Campbell Family Mental Health Research Institute, Centre for Addiction and Mental Health, Toronto, ON M5T 1R8, Canada
[5]Department of Pharmacology & Toxicology, University of Toronto, Toronto, ON M5S 1A1, Canada
[6]Lead contact
*Correspondence: etay.hay@camh.ca
https://doi.org/10.1016/j.isci.2025.112136

## SUMMARY

Major depressive disorder (depression) is associated with altered dendritic structure and function of cortical pyramidal neurons, due to decreased inhibition from somatostatin (SST) interneurons and loss of spines and associated synapses, as indicated in postmortem human studies. Dendrites mediate signal processing through synaptic integration and nonlinear properties including backpropagating action potentials and dendritic $Na^+$ spikes that enhance the neuron's computational power. However, it is currently unclear how depression-related dendritic changes impact signal integration. Here, we integrated human neuronal data of active dendritic properties and spine loss in depression into detailed computational models of human cortical microcircuits. We show that spine loss dampens signal response, worsening signal detection impairment than due to reduced SST interneuron inhibition alone. Furthermore, altered intrinsic properties due to spine loss abolished nonlinear dendritic signal integration and impaired recurrent microcircuit activity. Our study mechanistically links cellular changes in depression to impaired dendritic processing in human cortical microcircuits.

## INTRODUCTION

Major depressive disorder (depression) is associated with an altered cortical excitation-inhibition balance that disrupts signal processing.[1,2] Recent studies in humans and in chronically stressed rodents implicated altered dendritic mechanisms in cortical pyramidal (Pyr) neurons, due to reduced apical dendritic inhibition from somatostatin (SST) interneurons[1,3] and loss of dendritic spines and synapses.[4–7] We previously used detailed models of the human cortical microcircuits to link reduced SST interneuron inhibition in depression to functional impairments in signal detection.[8] However, the effects on dendritic input processing and the involvement of spine loss remain unclear.

Reduced SST interneuron inhibition in depression is supported by reduced expression of SST and other Gamma-aminobutyric acid (GABA) markers of SST interneurons in postmortem brain tissue from depression patients.[3,9] Similar changes in expression are also seen in chronic stress in rodents, which exhibit depressive and cognitive symptoms.[10] In support of a causal link, brain-wide silencing SST interneurons in rodents produced depression symptoms and cognitive impairments.[11] Chronic stress in rodents also induces a loss of spines in the basal and apical dendrites of Pyr neurons in the prefrontal cortex,[6] and a loss of synapses on spines in the dorsolateral prefrontal cortex was also found postmortem in depression patients.[7] Accordingly, application of pharmacology modulating $\alpha$5-$GABA_A$ receptors that SST interneurons target had antidepressant and pro-cognitive effects and also increased spine density in chronic stress in rodents.[6,12]

Dendrites contribute considerably to the computational power of neurons and microcircuits, by receiving and transforming signals through nonlinear properties.[13–16] Dendritic spines in excitatory Pyr neurons receive the majority of excitatory synaptic input[17] and also a considerable portion of inhibitory synaptic input.[18] The spines increase the surface area of the dendrites and thus the number of signals that can be integrated; they also affect the passive conductance and membrane capacitance and thus the excitability of the neuron.[19–21] Dendritic $Na^+$ channels allow for effective back-propagated action potentials (bAP) from the soma to the distal dendrites, which summate with incoming synapses to enhance dendritic processing and coincidence detection, as seen in rodents *in vitro* and *in silico*[22,23] and humans *in vitro*.[13] Dendritic ion channels also mediate local dendritic $Na^+$ spikes[22] that enable local dendritic non-linear computations, enhancing the neuron's computational power.[24] bAPs and dendritic $Na^+$ spikes can be inhibited by GABAergic inputs

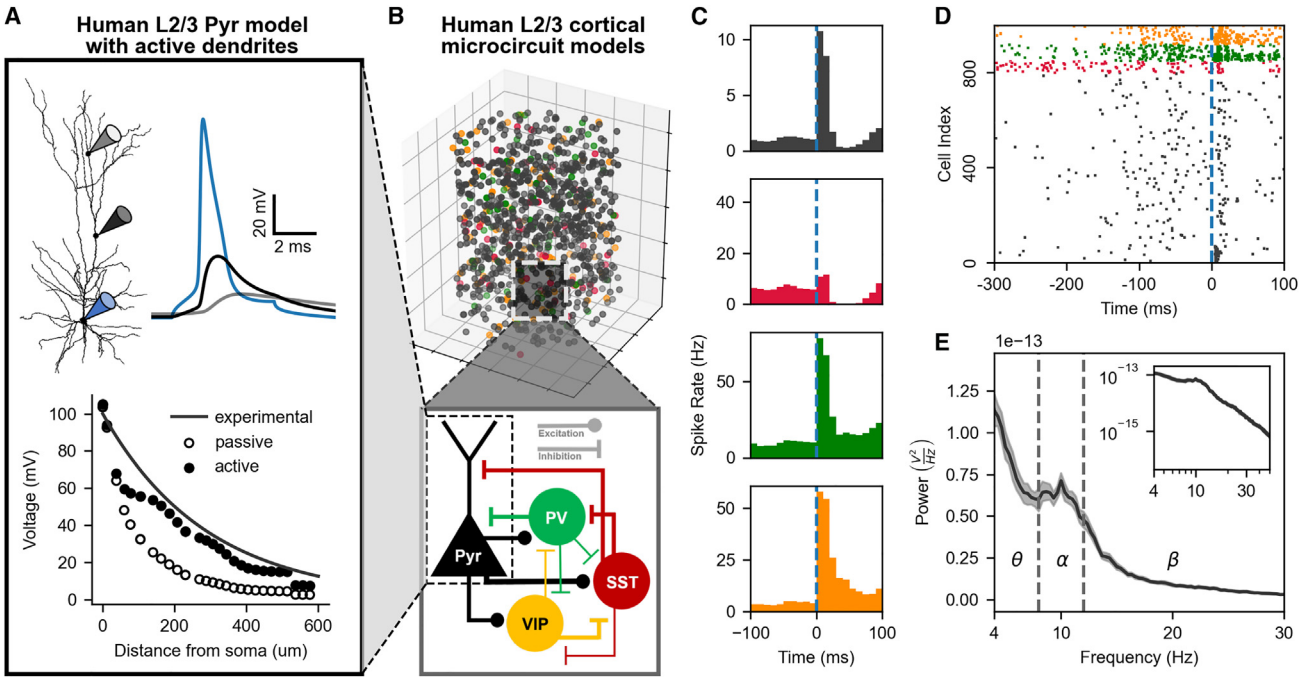


**Figure 1. Human L2/3 cortical microcircuit models with active dendrites**

(A) Model of human cortical L2/3 Pyr neuron with active dendrites and bAP. Top: human Pyr neuron morphology and simulated voltage at the soma (blue), 200 μm from soma (black) and 400 μm from soma (gray). Bottom: amplitude of bAP with distance from the soma in models with active and passive ($Na^+$ and $K^+$ channels blocked) dendrites. Solid black line shows the experimental fit from the literature.

(B) Models of human L2/3 cortical microcircuits included 1,000 neurons of the four key types: 800 Pyr, 50 SST, 70 parvalbumin-expression (PV), and 80 vasoactive intestinal peptide expression (VIP), distributed in a 500 × 500 × 950 $\mu m^3$ volume according to human dimensions. Bottom: schematic of the microcircuit connectivity between the different neuron types.

(C) Average peristimulus time histogram of microcircuit activity ($n$ = 100 simulated microcircuits). Vertical dashed line signifies onset of a brief stimulus (~5 ms).

(D) Example raster plot of microcircuit activity at baseline and response. Vertical dashed line signifies the stimulus onset.

(E) PSD of simulated EEG from the microcircuit ($n$ = 10 microcircuits). Dash lines separate different frequency bands. Inset shows the plot in log-log scale. Data points are shown as mean and shaded areas show 95% confidence intervals.

and therefore may be impacted by reduced inhibition and loss of synapses in depression.[25,26]

While rodent studies have linked reduced inhibition and spine loss to cognitive impairments,[6] a mechanistic link remains to be established, particularly in the human context. Nonlinear processing may differ between rodents and humans, as human dendrites are more complex and compartmentalized, and have larger diameters that result in higher thresholds for N-methyl-D-aspartate (NMDA) spikes.[14,27,28] In addition, human synapses are stronger with lower failure rates.[29–32] As such, the loss of synapses due to spine loss in depression may have larger or different effects in humans. We previously integrated human neuronal, synaptic, and connectivity data to generate detailed biophysical models of human cortical microcircuits in health and depression, and used them to link reduced SST interneuron inhibition with effects on cortical microcircuit activity and function.[8] Recent studies characterized dendritic bAP in human Pyr neurons,[13] providing important constraints to better simulate dendritic processing in health and depression.

In this study, we expanded our previous models to include human dendritic bAP properties, and spine loss in depression. Using these models, we studied the individual and combined effects of reduced SST interneuron inhibition and spine loss on cortical microcircuit baseline activity, signal response and signal detection error rates. Furthermore, we studied how changes in intrinsic properties due to spine loss can impact bAP-mediated dendritic processing on the cellular and microcircuit level.

## RESULTS

### Human L2/3 cortical microcircuit models with active dendrites

To investigate the impact of depression mechanisms on dendritic processing in human microcircuits, we first expanded our previous model of human cortical L2/3 Pyr neuron to include active dendrites with bAP. We uniformly distributed $K^+$ and $Na^+$ ion channels ($Na_T$: 0.0097 S/$cm^2$, $K_{V3\_1}$: 0.101 S/$cm^2$) on the apical dendrites, and generated models with bAP amplitudes similar to those recorded in human dendrites (Figure 1A). Compared to the passive dendrite, the active dendrites amplified the bAP amplitude by 194.5% ± 42.8%. In addition, the refitting of the Pyr models with active dendrites maintained a similar performance across all other electrophysiological features

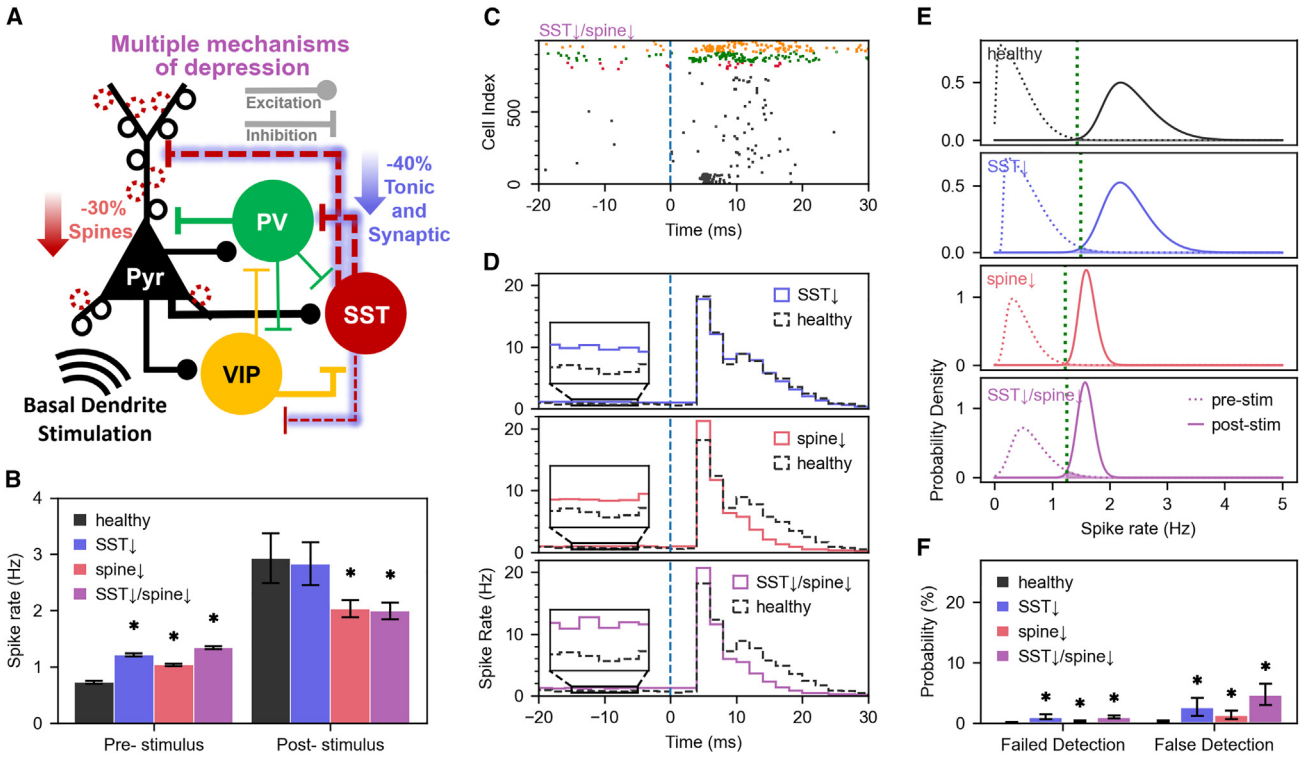


**Figure 2. Spine loss in depression dampens response to stimuli**

(A) Schematic of depression models for reduced SST inhibition (SST↓) and spine loss (spine↓).

(B) Average baseline and response spike rate of Pyr neurons in healthy and depression microcircuits.

(C) Example raster plot of SST↓/spine↓ microcircuit activity at baseline and response. Vertical dashed line signifies the onset of the stimulus.

(D) Average peristimulus time histogram of microcircuit activity in healthy vs. depression conditions ($n$ = 100 simulated microcircuits per condition).

(E) Distribution of pre-stimulus firing rates in 50-ms windows in example healthy and depression microcircuits ($n$ = 1,950 windows each) and distribution of firing rates 50 ms post-stimulus across 100 microcircuits ($n$ = 100 windows, bootstrapped 1,000 times). The vertical dotted line denotes the decision threshold of signal detection.

(F) Summary of false and failed stimulus detection rates in healthy and depression microcircuits ($n$ = 100 microcircuits per condition). Asterisk denotes $p < 0.05$ and large effect size, which were calculated using two-sample t test and Cohen's $d$. Data are represented as mean ± SD.

(step response, sag) as our previous model. We then integrated the new Pyr neuron models into our previous models of human L2/3 cortical microcircuits, and calibrated connection probabilities and background Ornstein-Uhlenbeck (OU) conductance[33] (see STAR Methods) to maintain the fit of average baseline firing rate and response profile in the different neuron types (Figures 1B–1D). The new models with active dendrites also maintained the prominent alpha peak in the simulated electroencephalogram (EEG) power spectral density (PSD) and improved on the previous models by having higher power in low-theta frequencies (4–6 Hz), thus better capturing the 1/f relationship seen in human resting-state EEG (Figure 1E).

## Effects of depression mechanisms on microcircuit processing

We used the models of human L2/3 cortical microcircuits with active dendrites to generate depression microcircuit models that included two key altered mechanisms: 40% reduced SST interneuron inhibition (SST↓), 30% spine loss in Pyr neurons (spine↓), and their combined effects (SST↓/spine↓, Figure 2A). Critically, spine loss involved the loss of excitatory and inhibitory synapses, as well as membrane surface area. Consistent with our previous findings, reduced SST inhibition in the expanded models significantly increased baseline activity (healthy: 0.72 ± 0.03 Hz; SST↓: 1.21 ± 0.03 Hz, 68% increase, $p < 0.05$, Cohen's $d$ = 13.9, Figure 2B) but had a negligible effect on the response (healthy: 2.9 ± 0.44 Hz; SST↓: 2.82 ± 0.39 Hz, 3% decrease, $p$ = 1.4e-6, Cohen's $d$ = −0.22, Figure 2B). Spine loss increased baseline activity as well, but to a lower extent (1.03 ± 0.02 Hz, 43% increase, $p < 0.05$, Cohen's $d$ = 12.2, compared to healthy). However, unlike SST interneuron inhibition loss, spine loss decreased the response rates (2.03 ± 0.15 Hz, 30% decrease, $p < 0.05$, Cohen's $d$ = 2.9, compared to healthy, Figures 2B–2D), primarily by decreasing recurrent activity that followed the bottom-up activation (~10–30 ms post-stimulus, Figure 2D). When both mechanisms were combined, the effect on baseline activity was slightly higher than SST↓, indicating a sublinear summed effect (1.33 ± 0.03 Hz, 85% increase, $p < 0.05$, Cohen's $d$ = 23.9, compared to healthy), whereas the response rates were decreased to an extent similar to the condition with only spine loss (1.99 ± 0.15 Hz, 31% decrease, $p < 0.05$, Cohen's $d$ = 2.9, compared to healthy, Figures 2B–2D).

**Table 1. Summary of the effects of reduced inhibition and spine loss on signal detection errors**

| | Failed detection | False detection |
|---|---|---|
| Healthy | 0.58 ± 0.2% | 1.70 ± 0.94% |
| SST↓ | 2.69 ± 0.53% | 9.15 ± 3.59% |
| spine↓ | 1.18 ± 0.31% | 5.21 ± 2.25% |
| spine↓/SST↓ | 4.25 ± 0.71% | 17.29 ± 4.31% |

To investigate the effects of depression mechanisms on signal detection error rates, we calculated the failed and false detection rates from the distribution of Pyr firing rate in 50 ms windows at baseline and during response (Figure 2E). In the SST↓ condition, the distribution of baseline rate was right-shifted, resulting in increased failed detection of signals (healthy: 0.58 ± 0.2%, SST↓: 2.69 ± 0.53%, $p < 0.05$, Cohen's $d = 5.0$, Figure 2F and Table 1) and false detection (healthy: 1.70 ± 0.94%, SST↓: 9.15 ± 3.59%, $p < 0.05$, Cohen's $d = 2.8$). In the spine↓ condition, there was a considerable left shift of the response rate distribution, and also a narrowing of both baseline and response distributions, which resulted in an overall increase in failed detection (1.18 ± 0.31%, $p < 0.05$, Cohen's $d = 2.1$, compared to healthy) and false detection (5.21 ± 2.25%, $p < 0.05$, Cohen's $d = 2.0$, compared to healthy), but to a lesser extent than in the SST↓ condition. In the case of SST↓ and spine↓ combined, the effects summated supra-linearly for both failed detection (spine↓/SST↓: 4.25 ± 0.71%, $p < 0.05$, Cohen's $d = 6.9$, compared to healthy; SST↓ only + spine↓ only: 3.87 ± 0.61%, $p < 0.05$, Cohen's $d = 0.57$, compared to spine↓/SST↓) and false detection (spine↓/SST↓: 17.29 ± 4.31%, $p < 0.05$, Cohen's $d = 5.0$, compared to healthy; SST↓ only + spine↓ only: 14.36 ± 4.24%, $p < 0.05$, Cohen's $d = 0.68$, compared to spine↓/SST↓) due to a combined right shift of the baseline rate distribution and left shift of the response spike rate distribution.

## Effects of different depression severities on microcircuit processing

We next investigated how different levels of reduced SST interneuron inhibition (20%, 40%, and 60%) and spine loss (15%, 22.5%, and 30%) impact cortical microcircuit activity and signal detection errors (Figure 3). Baseline activity increased linearly with either reduced SST interneuron inhibition or spine loss, with a similar slope regardless of the severity level of either. The effect was significantly above healthy for all levels above 20% reduced inhibition and 15% spine loss (15% spine↓/40% SST↓ compared to healthy: $p < 0.05$, Cohen's $d = 5.1$, 22.5% spine↓/20% SST↓ compared to healthy: $p < 0.05$, Cohen's $d = 7.8$, Figure 3A). In contrast, all levels of spine loss had a similar effect on response rates, irrespective of SST interneuron inhibition that had no effect on response activity (Figure 3B). For detection error rates, 15% spine loss had no effect above healthy levels except for high levels (60%) of reduced SST interneuron inhibition (failed detection: $p < 0.05$, Cohen's $d = 2.8$, false detection: $p < 0.05$, Cohen's $d = 2.6$, compared to healthy, Figures 3C and 3D), whereas for 22.5% and 30% spine loss the effect was significant even for small levels (20%) of the reduced SST interneuron inhibition, with a sublinear relationship for 30% spine loss (Figures 3C and 3D). The increase in error rates between 22.5% and 30% spine loss was greater than the increase between 15% and 22.5% spine loss, indicating a nonlinear relationship with increasing spine loss (Figures 3C and 3D).

## Spine loss in abolishes nonlinear dendritic integration

After characterizing the effect of the depression mechanisms on the microcircuit response to bottom-up inputs, we turned to investigate the effect of spine loss on dendritic integration with bAP (Figure 4A). The decreased membrane capacitance and leak conductance due to spine loss in depression resulted in abnormally large bAP amplitude (44.3 ± 10.9 mV; 261.6 ± 108.5% Figure 4B) in 3 of the 6 major paths from midway of the dendritic tree to the distal end (distance >250–300 μm from soma), due to decreases in dendrite diameters to <1.2 μm. These abnormally large bAPs also had decreased half-width (−5.4 ± 1.6 ms; −72.3 ± 12.1% Figure 4C). To investigate how these changes in bAP amplitude and half-width impact the integration of incoming dendritic synaptic inputs, we elicited postsynaptic potentials (PSPs) of increasing strength at 400 μm from the soma shortly after the peak of the bAP (6 ms after the somatic stimulation) and calculated the integral of the local dendritic voltage between 6 and 12 ms post-stimulus (Figure 4D). In the healthy condition, PSPs integrated nonlinearly with the bAP, exhibiting a sharp increase in dendritic depolarization beyond a certain magnitude of synaptic input. The non-linearity was abolished in the spine↓ condition (dendritic voltage integral for 0.0024 μS synaptic conductance relative to no synaptic input: healthy: 137.0 mV*ms, spine↓: 91 mV*ms, 33.6% decrease, Figure 4E). To investigate whether the nonlinear dendritic integration impacted the soma, we measured the peak voltage in the soma following the dendritic stimulation (between 10 and 14 ms post-stimulus). We similarly found a nonlinear increase in depolarization that was present in the healthy condition but not in the spine↓ condition, resulting in greater somatic excitation in the healthy neuron (somatic voltage for 0.0024 μS synaptic conductance relative to no synaptic input: healthy: 0.83 mV, spine↓: 0.54 mV, 35% decrease, Figure 4F).

We next investigated the effect of spine loss on dendritic input integration in the microcircuit by stimulating a population of 55 Pyr neurons with a similar protocol as aforementioned, with a suprathreshold somatic stimulus (t = 0 ms) and synaptic input at the distal apical dendrite (t = 6 ms) with varying activation strength (0–100 synapses, Figure 5A). The apical inputs generated a second peak in the peristimulus time histogram (PSTH) spiking response at around 10 ms after the somatic stimulation, and increased recurrent activity from the time of dendritic stimulation (6 ms) to 30 ms post-stimulus (Figures 5B and 5C). Across all numbers of dendritic synapses that we have simulated, depression microcircuits had reduced firing rates compared to healthy microcircuits (for example, 100 synapses: SST↓/spine↓: 5.81Hz ± 0.91 Hz, healthy: 10.7 Hz ± 1.95 Hz, $p < 0.05$, Cohen's $d = 3.2$, Figure 5D). Moreover, the gain of the response rate as a function of the number of apical synaptic inputs was reduced in depression (SST↓/spine↓: 4.15 ± 0.38 Hz/100 synapses, healthy: 8.77 ± 1.37 Hz/100 synapses, $p < 0.05$, Cohen's $d = 4.6$, Figure 5D).

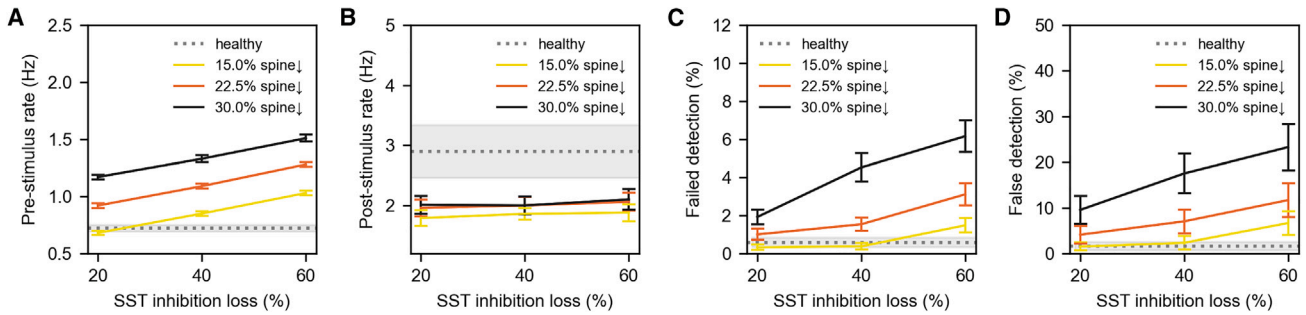


**Figure 3. Effects of different levels of SST interneuron inhibition and spine loss on firing and error rates**

(A) Pre-stimulus rates for microcircuits with different levels of SST interneuron inhibition and spine loss relative to healthy (horizontal dashed line).

(B–D) Same as (A) but for post-stimulus rates (B), failed detection (C), and false detection (D) of signals. Data points show mean ± SD.

## DISCUSSION

In this study, we linked altered dendritic mechanisms in depression with impaired signal integration in human neurons and cortical microcircuits. To overcome limitations of studying dendrites and microcircuits in the living human brain, we expanded our previous detailed computational models to reproduce human active dendritic properties of bAP and dendritic spine loss in depression. We demonstrated that spine loss impaired response firing, in contrast to reduced SST interneuron inhibition mainly affecting baseline firing. Furthermore, we showed that spine loss abolishes the non-linear synaptic integration mediated by bAP and thus impairs cortical recurrent activity. Our results with the expanded models differentiate effects of reduced SST interneuron inhibition and spine loss on dendritic signal processing in depression. These models can be used to refine corresponding EEG biomarkers[34] and enable more accurate estimation of the effects of recent depression pharmacology[35] that targets the apical dendrites.

Our findings of reduced response due to spine loss in depression can explain reduced cortical activity in patients during somatosensory response[36] and in cognitive tasks,[37–39] which was correlated with depression severity.[36] The decreased recurrent activity due to spine loss that we found could play a role in the reduced sustained neural activity in depression patients when processing positive emotional stimuli.[40] Our results may extend to diseases such as Alzheimer's disease[41] and schizophrenia,[42] where spine loss and reduced cortical activity during response[43] are also observed and are correlated with cognitive deficits.[44] We modeled spine loss according to rodent data in mild chronic stress, which is of a similar order of magnitude to the level of spine synapse loss in postmortem human tissues[6,7] although somewhat lower (rodent: 30%, human: 50%). A possible reason is that mild chronic stress is more similar to an early or induction stage of depression, with moderate spine loss.[45] Another reason may be that the human study[7] involved older subjects, with potentially fewer spines due to aging.[46] We used the rodent data as it was richer and enabled better constraints for spine loss in basal and apical dendrites and did not have the age confound that the human study had. Our neuron models were connected with several synaptic contacts according to previous studies (e.g., Pyr -> Pyr: 3 synapses, SST -> Pyr: 12 synapses).[29,47] To model spine loss, we decreased the number of synaptic contacts per connection to Pyr neurons, which was an independent from the connection probability parameter in our model. The partial loss of number of contacts thus did not incur a change in connection probability. While the connectivity changes underlying synapse loss are unclear and can alternatively be modeled as decreased connection probability between neuron types, our choice corresponded more directly to the available data. The net loss of synapses and change in the excitation/inhibition should be similar in either case, but future work can compare the effects of the different implementations. We modeled spine loss in terms of altered intrinsic properties of dendrites and did not model spines in detail, since the change in intrinsic properties sufficed to investigate the effects on overall dendritic integration, but future studies can use more detailed models of dendritic spines[48] to study how reduced spine density in depression impacts localized computations within spines.[49] Future studies can also examine the effects of reduced dendrite length and complexity, which were observed in restraint stress rodent model studies and suggested by studies of postmortem tissue of depression patients, which reported reduced microtubule-associated protein 2, a regulator of microtubule dynamics within cytoskeletons of neuronal dendrites that controls the length and structure of the dendrites.[7,50] However, these changes remain out of the scope of the current study due to lack of sufficient human data.

The abolishment of non-linear dendritic integration in spine loss resulted from abnormally large amplitudes of bAP, which shortened the dendritic bAP half-width and thus the summation time window with PSPs and also deactivated sodium channels that mediate nonlinear boosting of PSP.[51,52] Similar large amplitude bAP has been observed in rodents due to changes in dendritic sodium and potassium channels,[53] and here we demonstrate an alternative mechanism of decreased membrane capacitance and passive conductance due to spine loss. bAP has also been shown to mediate dendritic release of brain-derived neurotrophic factor,[54] a key transcription factor that is reduced in depression and plays a role in maintaining dendritic spines and SST expression.[55–57] Altered bAP in depression may therefore have further effects beyond the ones we have simulated. Our models reproduced bAP amplitudes, but the propagation of bAP was slower in our models than measured

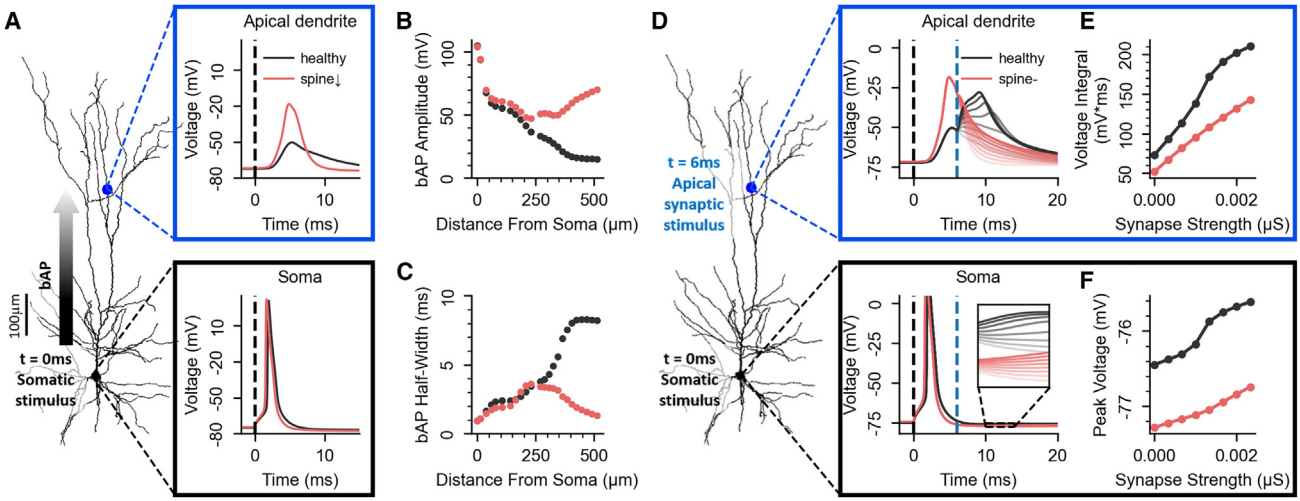


**Figure 4. Spine loss in depression impairs nonlinear dendritic integration with bAP**

(A) Simulation of a bAP traveling along the apical dendrite in a Pyr neuron in health (black) and depression (spine↓, red), showing voltage traces at distal apical dendrites (400 μm from soma, top) and at the soma (bottom).

(B) Amplitude of bAP at different distances from the soma.

(C) Half-width of bAP at different distances from the soma.

(D) Simulation of a bAP traveling along the apical dendrite in a Pyr neuron, coincident with incoming apical synaptic inputs of increasing strength, in health and depression. Plots show the voltage traces at the location of synaptic stimulation (400 μm from soma, top) and at the soma (bottom), with the opacity of the colors corresponding to the synapse strength. The inset shows the somatic voltage traces at 10–14 ms post-stimulus, analyzed in panel F.

(E) Integral of dendritic voltage over 6–12 ms post-stimulus in response to different synaptic strength, in health and depression.

(F) Peak voltage in the 10–14 ms window post-stimulus at the soma, in health and depression.

experimental values,[13] possibly due to the dendrites being more branched in the morphology we used.[58] However, the difference would mainly shift the relevant temporal delay of bAP and PSP summation, for which our spine loss results would hold as well. Future studies can look into using different morphologies to improve the propagation speed. We did not model bAP in the basal dendrites due to a lack of corresponding human data. We also did not model dendritic calcium spikes, which were shown to uniquely enable anti-coincidence detection of signals in humans,[13] because data of the ionic channel mechanisms by which these calcium spikes arise is not yet available. Our expanded models with active dendrites can improve identifying corresponding *in-silico* EEG biomarkers,[34] since bAP and dendritic currents significantly contribute to EEG signal.[59] Our models can also be used to improve the *in-silico* testing of recent pharmacology that targets SST interneuron inhibition pathway,[35] by estimating the pharmacology effects on dendritic integration.

## Limitations of the study

A large portion of the parameters in our models was constrained using human data, but for some parameters we used rodent data where human data are not yet available. These primarily included the firing rate of different interneuron types at baseline and response, and the properties of some synaptic connections. While there may be interspecies differences that could affect our results and some microcircuit properties such as oscillatory dynamics,[60] the activity of Pyr neurons, which make up majority of our microcircuit models, and the connections involving Pyr neurons were well constrained using human data.[29–31,61] Consequently, our models captured key properties of human resting-state EEG such as the alpha peak and the 1/f decay in the, providing a good validation and support for the model ability to capture key microcircuit dynamics. In addition, while our results provide predictions of the effects of reduced SST interneuron inhibition and spine loss in depression on cortical processing, these predictions remain to be verified by future experiments. As our ability to probe microcircuits in the living human brain is limited, an example possible validation could be achieved through corroborating our predicted changes in signal detection curves with performance data in patients.

We modeled our SST interneuron population as Martinotti interneurons since it is the most common type of SST interneurons, for which human data are also most readily available.[30,62] However, there are other subtypes of SST interneurons with distinct properties and molecular signatures and should be modeled in the future as data become available.[63,64] For example, non-Martinotti SST population expressing X94 preferentially target fast-spiking interneurons instead of the apical dendrites of Pyr neurons.[63] However, these SST interneurons are primarily located in deeper layers and are therefore outside of the scope of this study, but future studies could investigate the effects of reduced inhibition from these SST interneuron types. Importantly, our models reproduce the disynaptic loop involving Martinotti interneurons, which plays a key role in lateral inhibition, signal-gating and processing,[30,63,65] and is thus also implicated in depression deficits.[2,11] Future studies should also characterize the effect of reduced inhibition from SST interneurons in L5, where these interneurons are abundant and have

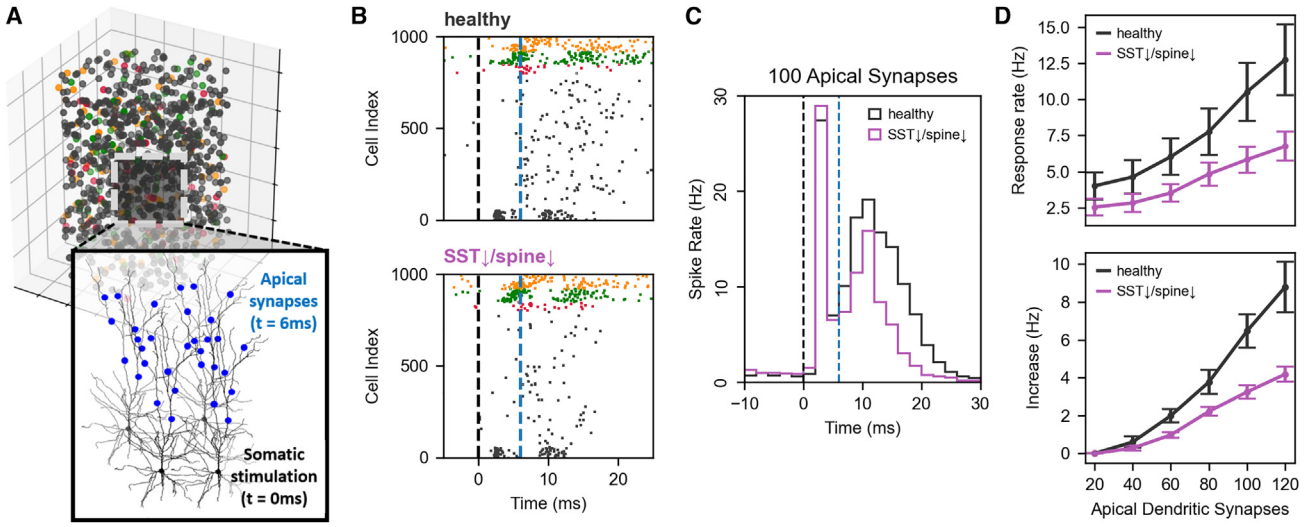


**Figure 5. Decreased nonlinear integration of signals in depression microcircuits**

(A) Schematic showing stimulation protocol of a microcircuit, where 55 Pyr neurons were stimulated at the soma, followed (t = 6 ms) by stimulation at the distal apical dendrites with varying activation strength (0–120 synapses).

(B) Example raster plots showing baseline and response to 100 apical dendritic synaptic inputs in healthy and depression (black: Pyr, red: SST, green: PV, yellow: VIP). Black and blue vertical dashed line show the start of somatic and dendritic stimulation, respectively.

(C) PSTH of baseline and response to somatic and distal apical stimulation with 100 synapses.

(D) Top: bootstrapped mean spike rate of Pyr neurons in response to somatic and apical synaptic stimulation, in healthy and depression microcircuits. Bottom: increase in mean spike rates relative to the case of 20 apical dendritic synapses, in healthy and depression microcircuits. Error bars show standard deviation.

larger morphologies and higher expression of SST neuropeptides and thus could have different effects.[66]

## RESOURCE AVAILABILITY

### Lead contact

Further information and requests for resources should be directed to and will be fulfilled by the lead contact, Etay Hay (etay.hay@camh.ca).

### Materials availability

This study did not generate new unique reagents.

### Data and code availability

- Simulation data reported in this paper will be shared by the lead contact upon request.
- All original code has been deposited at Zenodo and is publicly available as of the date of publication. DOIs are listed in the key resources table.
- Any additional information required to reanalyze the data reported in this paper is available from the lead contact upon request.

## ACKNOWLEDGMENTS

H.K.Y., F.M., and E.H. thank the Krembil Foundation for their generous funding support. H.K.Y. was also supported by Ontario Graduate Scholarship.

## AUTHOR CONTRIBUTIONS

Conception, H.K.Y., E.H., E.S., and T.D.P.; methodology, H.K.Y. and E.H.; software, H.K.Y., F.M., and E.H.; formal analysis, H.K.Y., F.M., and E.H.; investigation, H.K.Y., F.M., and E.H.; resources, E.H.; data curation, H.K.Y. and E.H.; writing – original draft, H.K.Y. and E.H.; writing – review & editing, H.K.Y., E.H., F.M., T.D.P., and E.S.; visualization, H.K.Y. and E.H.; supervision, E.H. and E.S.; project administration, E.H.; funding acquisition, E.H. and H.K.Y.

## DECLARATION OF INTERESTS

The authors declare no competing interests.

## STAR★METHODS

Detailed methods are provided in the online version of this paper and include the following:

- KEY RESOURCES TABLE
- EXPERIMENTAL MODEL AND STUDY PARTICIPANT DETAILS
- METHOD DETAILS
  - Human L2/3 Pyr neuron models with active dendrites
  - Human L2/3 microcircuit models
  - Simulated EEG
  - Simulating coincidence of bAP and synaptic input
  - Reduced SST interneuron inhibition depression microcircuit models
  - Spine loss depression microcircuit models
  - False/failed signal detection rates
- QUANTIFICATION AND STATISTICAL ANALYSIS

Received: September 13, 2024
Revised: December 23, 2024
Accepted: February 26, 2025
Published: March 3, 2025

## REFERENCES

1. Lissemore, J.I., Bhandari, A., Mulsant, B.H., Lenze, E.J., Reynolds, C.F., 3rd, Karp, J.F., Rajji, T.K., Noda, Y., Zomorrodi, R., Sibille, E., et al. (2018). Reduced GABAergic cortical inhibition in aging and depression. Neuropsychopharmacology *43*, 2277–2284.

2. Northoff, G., and Sibille, E. (2014). Why are cortical GABA neurons relevant to internal focus in depression? A cross-level model linking cellular, biochemical and neural network findings. Mol. Psychiatry *19*, 966–977.
3. Seney, M.L., Tripp, A., McCune, S., Lewis, D.A., and Sibille, E. (2015). Laminar and cellular analyses of reduced somatostatin gene expression in the subgenual anterior cingulate cortex in major depression. Neurobiol. Dis. *73*, 213–219.
4. Radley, J.J., Rocher, A.B., Miller, M., Janssen, W.G.M., Liston, C., Hof, P.R., McEwen, B.S., and Morrison, J.H. (2006). Repeated Stress Induces Dendritic Spine Loss in the Rat Medial Prefrontal Cortex. Cereb. Cortex *16*, 313–320.
5. Radley, J.J., Sisti, H.M., Hao, J., Rocher, A.B., McCall, T., Hof, P.R., McEwen, B.S., and Morrison, J.H. (2004). Chronic behavioral stress induces apical dendritic reorganization in pyramidal neurons of the medial prefrontal cortex. Neuroscience *125*, 1–6.
6. Bernardo, A., Lee, P., Marcotte, M., Mian, M.Y., Rezvanian, S., Sharmin, D., Kovačević, A., Savić, M.M., Cook, J.M., Sibille, E., and Prevot, T.D. (2022). Symptomatic and neurotrophic effects of GABAA receptor positive allosteric modulation in a mouse model of chronic stress. Neuropsychopharmacology *47*, 1608–1619.
7. Kang, H.J., Voleti, B., Hajszan, T., Rajkowska, G., Stockmeier, C.A., Licznerski, P., Lepack, A., Majik, M.S., Jeong, L.S., Banasr, M., et al. (2012). Decreased expression of synapse-related genes and loss of synapses in major depressive disorder. Nat. Med. *18*, 1413–1417.
8. Yao, H.K., Guet-McCreight, A., Mazza, F., Moradi Chameh, H., Prevot, T.D., Griffiths, J.D., Tripathy, S.J., Valiante, T.A., Sibille, E., and Hay, E. (2022). Reduced inhibition in depression impairs stimulus processing in human cortical microcircuits. Cell Rep. *38*, 110232.
9. Guilloux, J.-P., Douillard-Guilloux, G., Kota, R., Wang, X., Gardier, A.M., Martinowich, K., Tseng, G.C., Lewis, D.A., and Sibille, E. (2012). Molecular evidence for BDNF- and GABA-related dysfunctions in the amygdala of female subjects with major depression. Mol. Psychiatry *17*, 1130–1142.
10. Lin, L.C., and Sibille, E. (2015). Somatostatin, neuronal vulnerability and behavioral emotionality. Mol. Psychiatry *20*, 377–387.
11. Fee, C., Prevot, T.D., Misquitta, K., Knutson, D.E., Li, G., Mondal, P., Cook, J.M., Banasr, M., and Sibille, E. (2021). Behavioral deficits induced by somatostatin-positive GABA neuron silencing are rescued by alpha 5 GABA-A receptor potentiation. Int. J. Neuropsychopharmacol. *24*, 505–518. https://doi.org/10.1093/ijnp/pyab002.
12. Prevot, T.D., Sumitomo, A., Tomoda, T., Knutson, D.E., Li, G., Mondal, P., Banasr, M., Cook, J.M., and Sibille, E. (2021). Reversal of Age-Related Neuronal Atrophy by α5-GABAA Receptor Positive Allosteric Modulation. Cereb. Cortex *31*, 1395–1408. https://doi.org/10.1093/cercor/bhaa310.
13. Gidon, A., Zolnik, T.A., Fidzinski, P., Bolduan, F., Papoutsi, A., Poirazi, P., Holtkamp, M., Vida, I., and Larkum, M.E. (2020). Dendritic action potentials and computation in human layer 2/3 cortical neurons. Science *367*, 83–87.
14. Beaulieu-Laroche, L., Toloza, E.H.S., van der Goes, M.S., Lafourcade, M., Barnagian, D., Williams, Z.M., Eskandar, E.N., Frosch, M.P., Cash, S.S., and Harnett, M.T. (2018). Enhanced Dendritic Compartmentalization in Human Cortical Neurons. Cell *175*, 643–651.e14.
15. Hay, E., and Segev, I. (2015). Dendritic Excitability and Gain Control in Recurrent Cortical Microcircuits. Cereb. Cortex *25*, 3561–3571.
16. Beniaguev, D., Segev, I., and London, M. (2021). Single cortical neurons as deep artificial neural networks. Neuron *109*, 2727–2739.e3.
17. Liu, X.B., Zheng, Z.H., Xi, M.C., and Wu, C.P. (1991). Distribution of synapses on an intracellularly labeled small pyramidal neuron in the cat motor cortex. Anat. Embryol. *184*, 313–318.
18. Chen, J.L., Villa, K.L., Cha, J.W., So, P.T.C., Kubota, Y., and Nedivi, E. (2012). Clustered dynamics of inhibitory synapses and dendritic spines in the adult neocortex. Neuron *74*, 361–373.
19. Tsay, D., and Yuste, R. (2004). On the electrical function of dendritic spines. Trends Neurosci. *27*, 77–83.
20. Bekkers, J.M., and Häusser, M. (2007). Targeted dendrotomy reveals active and passive contributions of the dendritic tree to synaptic integration and neuronal output. Proc. Natl. Acad. Sci. USA *104*, 11447–11452.
21. Ichiyama, A., Mestern, S., Benigno, G.B., Scott, K.E., Allman, B.L., Muller, L., and Inoue, W. (2022). State-dependent activity dynamics of hypothalamic stress effector neurons. Elife *11*, e76832.
22. Larkum, M.E., Zhu, J.J., and Sakmann, B. (2001). Dendritic mechanisms underlying the coupling of the dendritic with the axonal action potential initiation zone of adult rat layer 5 pyramidal neurons. J. Physiol. *533*, 447–466.
23. Rapp, M., Yarom, Y., and Segev, I. (1996). Modeling back propagating action potential in weakly excitable dendrites of neocortical pyramidal cells. Proc. Natl. Acad. Sci. USA *93*, 11985–11990.
24. Gooch, H.M., Bluett, T., Perumal, M.B., Vo, H.D., Fletcher, L.N., Papacostas, J., Jeffree, R.L., Wood, M., Colditz, M.J., McMillen, J., et al. (2022). High-fidelity dendritic sodium spike generation in human layer 2/3 neocortical pyramidal neurons. Cell Rep. *41*, 111500.
25. Lowe, G. (2002). Inhibition of backpropagating action potentials in mitral cell secondary dendrites. J. Neurophysiol. *88*, 64–85.
26. Waters, J., Schaefer, A., and Sakmann, B. (2005). Backpropagating action potentials in neurones: measurement, mechanisms and potential functions. Prog. Biophys. Mol. Biol. *87*, 145–170.
27. Testa-Silva, G., Rosier, M., Honnuraiah, S., Guzulaitis, R., Megias, A.M., French, C., King, J., Drummond, K., Palmer, L.M., and Stuart, G.J. (2022). High synaptic threshold for dendritic NMDA spike generation in human layer 2/3 pyramidal neurons. Cell Rep. *41*, 111787.
28. Kalmbach, B.E., Hodge, R.D., Jorstad, N.L., Owen, S., de Frates, R., Yanny, A.M., Dalley, R., Mallory, M., Graybuck, L.T., Radaelli, C., et al. (2021). Signature morpho-electric, transcriptomic, and dendritic properties of human layer 5 neocortical pyramidal neurons. Neuron *109*, 2914–2927.e5.
29. Seeman, S.C., Campagnola, L., Davoudian, P.A., Hoggarth, A., Hage, T.A., Bosma-Moody, A., Baker, C.A., Lee, J.H., Mihalas, S., Teeter, C., et al. (2018). Sparse recurrent excitatory connectivity in the microcircuit of the adult mouse and human cortex. Elife *7*, e37349.
30. Obermayer, J., Heistek, T.S., Kerkhofs, A., Goriounova, N.A., Kroon, T., Baayen, J.C., Idema, S., Testa-Silva, G., Couey, J.J., and Mansvelder, H.D. (2018). Lateral inhibition by Martinotti interneurons is facilitated by cholinergic inputs in human and mouse neocortex. Nat. Commun. *9*, 4101.
31. Molnár, G., Rózsa, M., Baka, J., Holderith, N., Barzó, P., Nusser, Z., and Tamás, G. (2016). Human pyramidal to interneuron synapses are mediated by multi-vesicular release and multiple docked vesicles. Elife *5*, e18167.
32. Hunt, S., Leibner, Y., Mertens, E.J., Barros-Zulaica, N., Kanari, L., Heistek, T.S., Karnani, M.M., Aardse, R., Wilbers, R., Heyer, D.B., et al. (2023). Strong and reliable synaptic communication between pyramidal neurons in adult human cerebral cortex. Cereb. Cortex *33*, 2857–2878. https://doi.org/10.1093/cercor/bhac246.
33. Destexhe, A., Rudolph, M., Fellous, J.M., and Sejnowski, T.J. (2001). Fluctuating synaptic conductances recreate *in vivo*-like activity in neocortical neurons. Neuroscience *107*, 13–24.
34. Mazza, F., Guet-McCreight, A., Valiante, T.A., Griffiths, J.D., and Hay, E. (2023). In-silico EEG biomarkers of reduced inhibition in human cortical microcircuits in depression. PLoS Comput. Biol. *19*, e1010986.
35. Guet-McCreight, A., Chameh, H.M., Mazza, F., Prevot, T.D., Valiante, T.A., Sibille, E., and Hay, E. (2024). In-silico testing of new pharmacology for restoring inhibition and human cortical function in depression. Commun. Biol. *7*, 225.
36. Salustri, C., Tecchio, F., Zappasodi, F., Bevacqua, G., Fontana, M., Ercolani, M., Milazzo, D., Squitti, R., and Rossini, P.M. (2007). Cortical excitability and rest activity properties in patients with depression. J. Psychiatry Neurosci. *32*, 259–266.

37. Okada, G., Okamoto, Y., Morinobu, S., Yamawaki, S., and Yokota, N. (2003). Attenuated Left Prefrontal Activation during a Verbal Fluency Task in Patients with Depression. Neuropsychobiology *47*, 21–26.

38. Elliott, R., Baker, S.C., Rogers, R.D., O'Leary, D.A., Paykel, E.S., Frith, C.D., Dolan, R.J., and Sahakian, B.J. (1997). Prefrontal dysfunction in depressed patients performing a complex planning task: a study using positron emission tomography. Psychol. Med. *27*, 931–942.

39. Pu, S., Yamada, T., Yokoyama, K., Matsumura, H., Mitani, H., Adachi, A., Kaneko, K., and Nakagome, K. (2012). Reduced prefrontal cortex activation during the working memory task associated with poor social functioning in late-onset depression: Multi-channel near-infrared spectroscopy study. Psychiatry Res. *203*, 222–228.

40. Shestyuk, A.Y., Deldin, P.J., Brand, J.E., and Deveney, C.M. (2005). Reduced Sustained Brain Activity During Processing of Positive Emotional Stimuli in Major Depression. Biol. Psychiatry *57*, 1089–1096.

41. Dorostkar, M.M., Zou, C., Blazquez-Llorca, L., and Herms, J. (2015). Analyzing dendritic spine pathology in Alzheimer's disease: problems and opportunities. Acta Neuropathol. *130*, 1–19.

42. Glantz, L.A., and Lewis, D.A. (2000). Decreased Dendritic Spine Density on Prefrontal Cortical Pyramidal Neurons in Schizophrenia. Arch. Gen. Psychiatry *57*, 65–73.

43. Barch, D.M., Carter, C.S., Braver, T.S., Sabb, F.W., MacDonald, A., 3rd, Noll, D.C., and Cohen, J.D. (2001). Selective Deficits in Prefrontal Cortex Function in Medication-Naive Patients With Schizophrenia. Arch. Gen. Psychiatry *58*, 280–288.

44. Akram, A., Christoffel, D., Rocher, A.B., Bouras, C., Kövari, E., Perl, D.P., Morrison, J.H., Herrmann, F.R., Haroutunian, V., Giannakopoulos, P., and Hof, P.R. (2008). Stereologic estimates of total spinophilin-immunoreactive spine number in area 9 and the CA1 field: Relationship with the progression of Alzheimer's disease. Neurobiol. Aging *29*, 1296–1307.

45. Mineur, Y.S., Belzung, C., and Crusio, W.E. (2006). Effects of unpredictable chronic mild stress on anxiety and depression-like behavior in mice. Behav. Brain Res. *175*, 43–50.

46. Dickstein, D.L., Weaver, C.M., Luebke, J.I., and Hof, P.R. (2013). Dendritic spine changes associated with normal aging. Neuroscience *251*, 21–32.

47. Ramaswamy, S., Courcol, J.D., Abdellah, M., Adaszewski, S.R., Antille, N., Arsever, S., Atenekeng, G., Bilgili, A., Brukau, Y., Chalimourda, A., et al. (2015). The neocortical microcircuit collaboration portal: a resource for rat somatosensory cortex. Front. Neural Circuits *9*, 44.

48. Eyal, G., Verhoog, M.B., Testa-Silva, G., Deitcher, Y., Benavides-Piccione, R., DeFelipe, J., de Kock, C.P.J., Mansvelder, H.D., and Segev, I. (2018). Human Cortical Pyramidal Neurons: From Spines to Spikes via Models. Front. Cell. Neurosci. *12*, 181.

49. Yuste, R. (2011). Dendritic Spines and Distributed Circuits. Neuron *71*, 772–781.

50. DeGiosio, R.A., Grubisha, M.J., MacDonald, M.L., McKinney, B.C., Camacho, C.J., and Sweet, R.A. (2022). More than a marker: potential pathogenic functions of MAP2. Front. Mol. Neurosci. *15*, 974890.

51. London, M., and Häusser, M. (2005). Dendritic computation. Annu. Rev. Neurosci. *28*, 503–532.

52. Larkum, M.E., and Nevian, T. (2008). Synaptic clustering by dendritic signalling mechanisms. Curr. Opin. Neurobiol. *18*, 321–331.

53. Golding, N.L., Kath, W.L., and Spruston, N. (2001). Dichotomy of Action-Potential Backpropagation in CA1 Pyramidal Neuron Dendrites. J. Neurophysiol. *86*, 2998–3010.

54. Kuczewski, N., Porcher, C., Ferrand, N., Fiorentino, H., Pellegrino, C., Kolarow, R., Lessmann, V., Medina, I., and Gaiarsa, J.L. (2008). Backpropagating Action Potentials Trigger Dendritic Release of BDNF during Spontaneous Network Activity. J. Neurosci. *28*, 7013–7023.

55. Tripp, A., Oh, H., Guilloux, J.P., Martinowich, K., Lewis, D.A., and Sibille, E. (2012). Brain-Derived Neurotrophic Factor Signaling and Subgenual Anterior Cingulate Cortex Dysfunction in Major Depressive Disorder. Am. J. Psychiatry *169*, 1194–1202.

56. Oh, H., Piantadosi, S.C., Rocco, B.R., Lewis, D.A., Watkins, S.C., and Sibille, E. (2019). The Role of Dendritic Brain-Derived Neurotrophic Factor Transcripts on Altered Inhibitory Circuitry in Depression. Biol. Psychiatry *85*, 517–526.

57. Vigers, A.J., Amin, D.S., Talley-Farnham, T., Gorski, J.A., Xu, B., and Jones, K.R. (2012). Sustained expression of brain-derived neurotrophic factor is required for maintenance of dendritic spines and normal behavior. Neuroscience *212*, 1–18.

58. Vetter, P., Roth, A., and Häusser, M. (2001). Propagation of Action Potentials in Dendrites Depends on Dendritic Morphology. J. Neurophysiol. *85*, 926–937.

59. Reimann, M.W., Anastassiou, C.A., Perin, R., Hill, S.L., Markram, H., and Koch, C. (2013). A Biophysically Detailed Model of Neocortical Local Field Potentials Predicts the Critical Role of Active Membrane Currents. Neuron *79*, 375–390.

60. Cardin, J.A. (2018). Inhibitory interneurons regulate temporal precision and correlations in cortical circuits. Trends Neurosci. *41*, 689–700.

61. Teleńczuk, B., Dehghani, N., Le Van Quyen, M., Cash, S.S., Halgren, E., Hatsopoulos, N.G., and Destexhe, A. (2017). Local field potentials primarily reflect inhibitory neuron activity in human and monkey cortex. Sci. Rep. *7*, 40211.

62. 2010 Allen Institute for Brain Science. Allen Human Brain Atlas. human.brain-map.org.

63. Scheyltjens, I., and Arckens, L. (2016). The Current Status of Somatostatin-Interneurons in Inhibitory Control of Brain Function and Plasticity. Neural Plast. *2016*, 8723623.

64. Urban-Ciecko, J., and Barth, A.L. (2016). Somatostatin-expressing neurons in cortical networks. Nat. Rev. Neurosci. *17*, 401–409.

65. Silberberg, G., and Markram, H. (2007). Disynaptic Inhibition between Neocortical Pyramidal Cells Mediated by Martinotti Cells. Neuron *53*, 735–746.

66. Banovac, I., Sedmak, D., Esclapez, M., and Petanjek, Z. (2022). The Distinct Characteristics of Somatostatin Neurons in the Human Brain. Mol. Neurobiol. *59*, 4953–4965.

67. Van Geit, W., Gevaert, M., Chindemi, G., Rössert, C., Courcol, J.D., Muller, E.B., Schürmann, F., Segev, I., and Markram, H. (2016). BluePyOpt: Leveraging Open Source Software and Cloud Infrastructure to Optimise Model Parameters in Neuroscience. Front. Neuroinform. *10*, 17.

68. Carnevale, N.T., and Hines, M.L. (2006). The NEURON Book (Cambridge University Press, Cambridge). https://doi.org/10.1017/CBO9780511541612.

69. Hagen, E., Næss, S., Ness, T.V., and Einevoll, G.T. (2018). Multimodal Modeling of Neural Network Activity: Computing LFP, ECoG, EEG, and MEG Signals With LFPy 2.0. Front. Neuroinformatics *12*, 92.

70. Hay, E., Hill, S., Schürmann, F., Markram, H., and Segev, I. (2011). Models of Neocortical Layer 5b Pyramidal Cells Capturing a Wide Range of Dendritic and Perisomatic Active Properties. PLoS Comput. Biol. *7*, e1002107.

71. Hay, E., Schürmann, F., Markram, H., and Segev, I. (2013). Preserving axosomatic spiking features despite diverse dendritic morphology. J. Neurophysiol. *109*, 2972–2981.

72. Ponce, M., Van Zon, R., Northrup, S., Gruner, D., Chen, J., Ertinaz, F., Fedoseev, A., Groer, L., Mao, F., Mundim, B.C., et al. (2019). Deploying a Top-100 Supercomputer for Large Parallel Workloads: the Niagara Supercomputer. In Proceedings of the Practice and Experience in Advanced Research Computing on Rise of the Machines (learning) (Association for Computing Machinery, New York, NY, USA), pp. 1–8. https://doi.org/10.1145/3332186.3332195.

73. Mohan, H., Verhoog, M.B., Doreswamy, K.K., Eyal, G., Aardse, R., Lodder, B.N., Goriounova, N.A., Asamoah, B., B Brakspear, A.B.C., Groot, C., et al. (2015). Dendritic and Axonal Architecture of Individual Pyramidal Neurons across Layers of Adult Human Neocortex. Cereb. Cortex *25*, 4839–4853.

74. Fuhrmann, G., Segev, I., Markram, H., and Tsodyks, M. (2002). Coding of temporal information by activity-dependent synapses. J. Neurophysiol. *87*, 140–148.

75. Mäki-Marttunen, T., Krull, F., Bettella, F., Hagen, E., Næss, S., Ness, T.V., Moberget, T., Elvsåshagen, T., Metzner, C., Devor, A., et al. (2019). Alterations in Schizophrenia-Associated Genes Can Lead to Increased Power in Delta Oscillations. Cereb. Cortex *29*, 875–891.

76. Bryson, A., Hatch, R.J., Zandt, B.J., Rossert, C., Berkovic, S.F., Reid, C.A., Grayden, D.B., Hill, S.L., and Petrou, S. (2020). GABA-mediated tonic inhibition differentially modulates gain in functional subtypes of cortical interneurons. Proc. Natl. Acad. Sci. USA *117*, 3192–3202.

77. Moradi Chameh, H., Rich, S., Wang, L., Chen, F.D., Zhang, L., Carlen, P.L., Tripathy, S.J., and Valiante, T.A. (2021). Diversity amongst human cortical pyramidal neurons revealed via their sag currents and frequency preferences. Nat. Commun. *12*, 2497.

78. Scimemi, A., Andersson, A., Heeroma, J.H., Strandberg, J., Rydenhag, B., McEvoy, A.W., Thom, M., Asztely, F., and Walker, M.C. (2006). Tonic GABAA receptor-mediated currents in human brain. Eur. J. Neurosci. *24*, 1157–1160.

79. Gentet, L.J., Kremer, Y., Taniguchi, H., Huang, Z.J., Staiger, J.F., and Petersen, C.C.H. (2012). Unique functional properties of somatostatin-expressing GABAergic neurons in mouse barrel cortex. Nat. Neurosci. *15*, 607–612.

80. Yu, J., Hu, H., Agmon, A., and Svoboda, K. (2019). Recruitment of GABAergic Interneurons in the Barrel Cortex during Active Tactile Behavior. Neuron *104*, 412–427.e4.

81. Welch, P. (1967). The use of fast Fourier transform for the estimation of power spectra: A method based on time averaging over short, modified periodograms. IEEE Trans. Audio Electroacoust. *15*, 70–73.

## STAR★METHODS

### KEY RESOURCES TABLE

| REAGENT or RESOURCE | SOURCE | IDENTIFIER |
|---|---|---|
| Software and algorithms | | |
| Python 3.10 | Python Software Foundation | https://www.python.org/ |
| BluePyOpt | Van Geit et al.[67] | https://github.com/BlueBrain/BluePyOpt |
| NEURON 7.7 | Carnevale and Hines[68] | https://neuron.yale.edu/neuron/ |
| LFPy | Hagen et al.[69] | https://lfpy.readthedocs.io/en/latest/# |
| Human L2/3 microcircuit models with active Pyr neuron dendrites and simulation code | This paper | https://doi.org/10.5281/zenodo.12575278 |

### EXPERIMENTAL MODEL AND STUDY PARTICIPANT DETAILS

This section does not apply to our study as no new samples were collected.

### METHOD DETAILS

#### Human L2/3 Pyr neuron models with active dendrites

Following similar methods as in our previous work,[8] we generated multicompartmental conductance-based single neuron models for Pyr neurons with active dendrites using BluePyOpt.[67] Our models used reconstructed morphologies of human neurons from the Allen Institute.[62] We refitted the firing and passive electrophysiological features as our previous work[8] together with bAP amplitude features. To fit the bAP in the Pyr neuron, we injected a 1.0 mA current at the soma for 5 ms to elicit somatic action potentials and fitted the bAP amplitude along the apical dendrite at distances of 200 μm and 400 μm from the soma according to literature values (200 μm: ∼60mV, 400 μm: ∼15mV).[13] We distributed $Na_T$ and $K_{v3\_1}$ channels uniformly in the apical dendrites. $I_h$ channel was distributed with a sigmoidal function with the absolute distance from the soma:

$$g_H = g_h, g_{soma}\left(0.5 + \left(\frac{30}{1+\exp\left(\frac{x_{absolute} - 350}{-99}\right)}\right)\right) \quad \text{(Equation 1)}$$

Apical dendritic $Na_T$ kinetics parameters were the same as the axonal parameters based on past work[70,71] ($Vshift_m = 0$, $Vshift_h = 10$, $Slope_m = 9$, and $Slope_h = 6$). We used the same Pyr neuron morphology as our previous models, from the Allen Brain Atlas.[62] To run the model optimization, we used parallel computing clusters on SciNet[72] with 280 processors. The optimization used a population size of 280 over 400 generations for an approximate total runtime of 6 hours.

#### Human L2/3 microcircuit models

We integrated the new Pyr neuron model into our previous models of human cortical L2/3 microcircuits,[8] comprised of 1000 neurons (800 Pyr, 50 SST, 70 PV, and 80 VIP) distributed within a 500x500x950 $\mu m^3$ volume (250 to 1200 μm below pia, spanning L2/3[73]). The microcircuit models included α-Amino-3-hydroxy-5-methyl-4-isoxazolepropionic acid (AMPA)/NMDA and $GABA_A$ synaptic mechanisms,[15,74,75] tonic inhibition,[76] and were driven by random OU background inputs.[33] The models were constrained with human data of neuronal firing and passive properties for each of the neuron types, synaptic properties for most of the connection types, cell proportions, and *in vivo* baseline firing rate in Pyr neurons, where synaptic and connectivity properties for which human data was not available were constrained with primate or rodent data (see further detail in Yao et al. 2022).

PV and VIP interneuron models remained unchanged from our previous models. Previously, SST and Pyr models were fitted in a two-step process to individually fit the passive and active features. In the current work, we refitted the SST and Pyr models in a single step, fitting both the passive and active properties and using the BluePyOpt tool,[67] to maintain consistency with the methodology of the PV and VIP models. Synaptic connections targeting the new Pyr and SST neuron models were refitted to reproduce similar average amplitude as our previous models.[8] Tonic inhibition was re-estimated with the new Pyr neuron model with active dendrites following the same methods as previously,[8,77,78] resulting in a similar value (previous: 0.938 mS/cm$^2$, current: 0.994 mS/cm$^2$). We refitted the resulting microcircuits with new Pyr neuron and SST interneuron models to reproduce average *in vivo* firing rates across cell types[61,79,80] during baseline as in our previous models,[8] by adjusting the microcircuit connection probability and synaptic

conductance, and the strengths of OU background inputs (Below Table). To reproduce average spike rates and dynamics during response to a brief stimulus as in our previous models, we stimulated 70 Pyr neurons with 7 basal dendritic synapses (t: 2 - 3ms, g: 3 μS), 30 PV interneurons were with 10 dendritic synapses (t: 0 – 3 ms, g: 3 μS) and 45 VIP interneurons were with 10 dendritic synapses (t: 0 – 6 ms, g: 3 μS). Microcircuit models were simulated using NEURON[68] and LFPy.[69]

**Parameter changes relative to the previous model**

| | PYR | SST | PV | VIP |
|---|---|---|---|---|
| Synaptic conductance (pS) | | | | |
| PYR | 0.0000848 | −0.000044 | 0 | 0.00002 |
| SST | 0.000416 | 0.00008 | 0.00012 | 0 |
| PV | 0.00070166 | 0.00009 | 0.00012 | 0.00008 |
| VIP | 0 | 0.00006 | 0.00011 | 0.00008 |
| Connection probability (%) | | | | |
| PYR | 0 | −0.05 | 4.3 | 2 |
| SST | 0 | 0 | 6 | 12 |
| PV | 1.6 | −1 | −3 | 0 |
| VIP | 0 | −10 | 4 | −2 |
| OU conductance (pS) | 0.0000023 | 0.0000117 | −0.000078 | −0.0000012 |

For synaptic conductance and connection probability, rows correspond to the presynaptic neuron and columns correspond to the postsynaptic neuron.

## Simulated EEG

Using LFPy, we computed dipole moment from transmembrane currents within each cell in the microcircuit and generated the EEG timeseries using a four sphere volume conductor model with an EEG electrode placed directly above the circuit.[34,69] EEG PSD was calculated using Welch's method with a Hanning window of 3 seconds.[81]

## Simulating coincidence of bAP and synaptic input

We stimulated the soma with a step current of 0.7 mA for 2 ms to elicit a somatic action potential, and 6 ms after the somatic stimulation we followed by stimulation of a synapse on the apical dendrite (400 μm from the soma) with varying conductance strength (0 – 0.0024 μS). As a corresponding protocol of coincident somatic and apical inputs in the microcircuit simulations, we stimulated 55 Pyr neurons with 7 somatic synapses (t: 0 – 1 ms, g: 3 μS) to induce spikes for bAP, and 20 - 120 distal apical dendritic synapses (t: 6 – 7 ms, g: 0.3 μS). We activated less Pyr neurons than in the brief stimulus paradigm (see above) since in the coincidence paradigm the activation was in the soma rather dendrites, and was sufficient for generating moderate recurrent activity within the microcircuit, without under-activating or over-activating the circuit. To balance the microcircuit response, as in the simulations of brief stimulus response, we also stimulated 20 PV neurons with 10 dendritic synapses (t: 0 – 3 ms, g: 3 μS), and 38 VIP neurons with 10 dendritic synapses (t: 0 – 5 ms, g: 3 μS).

## Reduced SST interneuron inhibition depression microcircuit models

We used our previous models of depression microcircuits,[8] with 40% decreased SST interneuron synaptic and tonic inhibition, based on expression studies in post-mortem brain tissue of depression patients.[3] When decreasing the tonic inhibition, the calculation of the relative contribution of each interneuron type to the total tonic inhibitory input was now refined to also account for the average firing rates of each interneuron type.

## Spine loss depression microcircuit models

We modelled 30% spine density loss in the apical and basal dendrites of Pyr neurons, according to studies in rodents under chronic stress and in post-mortem human tissue,[6,7] by reducing the membrane capacitance and passive conductance due to spines in the apical and basal dendrites by 30% (equivalent to 15% of the total dendritic membrane capacitance and passive conductance, assuming a doubling of the surface area. i.e. an additional 1 μf/cm$^2$, for spine membrane area compensation[8]). To account for the loss of synapses due to spine loss, we reduced the number of synaptic contact points in connections that target Pyr neurons: as 80% of excitatory synapses and 30% of inhibitory synapses target spines,[17,18] we reduced contact points in Pyr→Pyr connections by ∼24% (from 3 to 2, due to the number of contacts being a discrete number, we rounded the experimental average to the closest number of contacts lost), and inhibitory synapses onto pyr by ∼9% (SST→Pyr connections from 12 to 10, and PV→Pyr connections from 17 to 15). In addition, the tonic inhibition of the Pyr neuron dendrites was reduced by 9%, and the conductance of excitatory OU processes on the Pyr neuron dendrites was reduced by 24%.

### False/failed signal detection rates

We calculated the error rates in stimulus detection by calculating the distribution of baseline firing rates of all Pyr neurons per circuit (sliding windows of 50 ms in 1 ms steps over 2 seconds pre-stimulus, for a total of 1950 windows), and the distribution of post-stimulus spike rates of all Pyr neurons in the 5 – 55 ms window post-stimulus across 100 randomized microcircuits (bootstrapped across all circuits, n = 1000 samples). The intersection point between the two distributions was set as the stimulus detection threshold. The probability of false detection was calculated by the integral of the pre-stimulus distribution above the detection threshold divided by the integral of the entire pre-stimulus distribution, and the probability of failed detection by the integral of the post-stimulus distribution below the detection threshold divided by the integral of the entire post-stimulus distribution.

## QUANTIFICATION AND STATISTICAL ANALYSIS

For all figures, we calculated statistical significance using two-sample t-test ($p < 0.05$), and effect size using Cohen's $d$ (the difference in means divided by the pooled standard deviation). Asterisk in figures denotes $p < 0.05$ and large effect size. For EEG simulations in Figure 1E, data points are shown as mean and shaded areas show 95% confidence intervals, n = 10 randomized microcircuits. For all other figures, n = 100 randomized microcircuits were used, and all data points are shown as mean ± standard deviation.